# Comparison of Atomistic and Phase Field Descriptions of [001] Symmetric Tilt Grain Boundary in Ni

E Ngenzi, S Queyreau

# Comparison of Atomistic and Phase Field Descriptions of [001] Symmetric Tilt Grain Boundary in Ni

E. Ngenzi [1] and S. Queyreau[1*]

[1] *Universit Sorbonne Paris Nord, LSPM-CNRS, UPR 3407, 93430 Villetaneuse, France*

## Abstract

During thermomechanical treatments, polycrystalline microstructures undergo a complex and dynamic evolution for which no real predictive model exists. We propose here to combine phase field simulations and molecular dynamics simulations to eventually fill this gap. We employ The Phase Field model of Admal and cowrokers [Int. J. Plast. 2018], which is derived from the so-called Kobayachi-Warren-Carter model, and is connected to crystal plasticity to include the mutual interactions of grain boundary migration with the presence of crystal dislocations. In the model, the grain boundary is itself a distribution of geometrically necessary dislocations. Comparison with atomistic data, shows that this PF model naturally captures some key features required to predict microstructure evolutions, such as grain boundary energy, shear coupling effect and even some mobility trends under the application of a driving force to migration. At the end of the paper, a (semi-) analytical model is proposed to quantitatively connect the phase field simulations to the reference Molecular Dynamics data.


## I. INTRODUCTION

Use of thermomechanical treatments is a classical and efficient way to taylor polycrystalline materials properties -in particular mechanical properties- to a given application. During a single or a sequence of treatments the microstructure evolves sometimes dramatically in an highly anisotropic and non-linear manner. This apparent complexity is commonly associated to the multiplicity of elementary mechanisms that are occurring simultaneously and maybe associated to different length- and times-scales [1, 2]. At the center of microstructural evolution is the normal motion of grain boundaries, but this migration depends upon the GB nature and may be accompanied by GB shear coupling, grain rotation, dislocation polygonalization etc... Ultimately and despite decades of efforts in that direction, there is to date no predictive tool capable of predicting quantitatively the evolution of polycrystalline microstructures. Trail-and-error strategies provide a practical solution but eventually limit microstructure engineering.

In this context, a multiscale simulation strategy could provide such a predictive tool but face several challenges [3, 4]. A first challenge relies on the fact that many GB properties are


* sylvain.queyreau@cnrs.fr

strongly depending upon the GB type and atomic structure, but the the atomic-structure-property relationship remain mostly poorly known, still to date. These details can only be addressed through the rare TEM high resolution analysis or atomistic data, and real microstructures contain virtually an infinite number of grain boundary type and orientation. Great care has been paid to the construction of the initial atomic configuration for the ground state [5, 6] or how to properly orient a bicrystal in order to study more complex GB geometry [7] encompassing asymmetrical GB and mixed tilt-twist character for which less data is available. These technical developments allow for systematic studies embracing the large variety of GB types and structures [8–12]. As a result of these studies, the complexity of the GB properties was set in the spotlight, and few attempts could rationalize some GB properties as function of the 5D dof for GB geometry [11]. GB migration as observed in MD was ca be categorized into a handful of various velocity function with respect to its temperature dependence [8–10]. The velocity trends are however not always consistent or monotonous [9, 10]. Since quantifying with precision the details of atomic processes at play during migration is a daunting task, the underlying kinetics of GB migration were successfully quantified in direct connection to the atomistic details in a handful of studies [13–16]. When comparing to the apparent complexity of lower order defects such as dislocations, it is surprising that so few features are shared among GB.

The mesoscale part of this multiscale approach is facing different challenges. First, at the scale of the microstructure, the mesoscale formalism chosen -among those available- needs to be able to account for a list of key mechanisms for GB migration in interaction with dislocation activity within the grains mentioned above. In this context, the Phase Field (PF) model initially proposed by Kobayachi-Warren-Carter (KWC) [17–19] was among the first attempt at including GB migration driven by curvature, crystal rotation. This diffuse GB model has been ever since extensively used and analysed [18–21], with in particular the path towards its analytical resolution through formal expansion analysis [20]. The KWC however lacks the connection to crystal dislocation interplay, and a couple of extensions of the KWC model addressing this limitation have been proposed approximately at the same time [22, 23]. Both approaches exploit the kinematic equivalency of GB in terms of crystalline defects to connect with a more classical crystal plasticity framework. The first extension proposed by Ask and coworker [22] consider GB as a source of lattice curvature and connect the KWC model to a Cosserat generalized continuum framework. The second alternative proposed by

Admal and coworker [23], describes GB in terms of GND distributions. Both approaches are perfectly valid choices to incorporate all the requires ingredients and mechanism for microstructure evolution.

The last challenge of this multiscale approach is obviously to make it quantitative to become truly predictive. In particular, the PF has to retain the key physical insights from atomistics regarding the GB properties and GB migration. However, MD and PF approaches solve a different physics. The PF makes use of two continuous fields: the crystal rotation $\theta$ and the lattice order $\phi$. Although, one could probably map these fields to the MD data using some arbitrary metric e.g. centrosymmetry parameter [24], these fields are the by-product of atomic interactions, and there is no guarantee that a clear link exist between these field and the physics simulated in MD. Few attempts exist in the litterature to connect PF to atomistic data [25, 26], and the task has been proved to be challenging.

In this paper, we compare the description of GB from the Admal et al. phase field model to atomistic data that will act as reference data, in order to devise a path to quantitatively connect the two approaches. For this, we will focus on symmetric tilt grain boundaries, as PF field are classically in 2D, in a pure Ni system for which extensive data exist and act as a model material for other fcc metals with intermediate stacking fault energy value. In the remainder of the paper, the first section first presents the details of the atomistic configurations and recall the specifics of Phase Field model model of Admal et al. Section two compares the results obtained with MD and PF on these four fundamental features GB: i) GB structure, ii) GB energy and and iv) GB migration. Finally, in the final discussion, we proposed a way to quantitatively parametrize the PF from atomistic data through a (semi) analytical solve of both the 1D KWC and the 1D Admal's models, paving the way to more quantitative PF simulations in the future.

## II. METHODS

### A. Molecular Dynamics simulations

Here, we present the results regarding STGB from a larger atomistic study in [12]. The systematic study of GB type is made easier by choosing a bicrystalline geometry [8, 10] as shown in figure 1. A plane GB is inserted in the center of the atomistic box, and Free

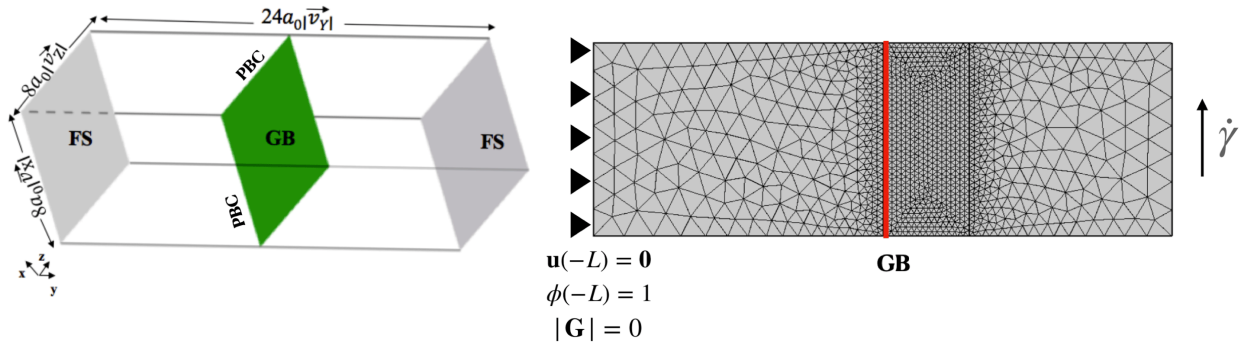


Figure 1. The simulation setup used in molecular dynamics simulations in which $\vec{v}_X$,$\vec{v}_Y$ and $\vec{v}_Z$ stand for the CSL vectors along the X, Y and Z directions respectively and $a_0$ is the lattice parameter. Free surface (FS) are shown in a grey colour, the Periodic boundary conditions (PBC) are applied on remaining sides and the Grain Boundary (GB) is shown in green colour [12]. To the right is a meshed phase field bi-crystalline domain in which a grain boundary is shown in red.

Surface (FS) are applied along the $y$ axis and Periodic Boundary Conditions (PBC) are applied on the other two simulation axii. The box dimension and orientation must be adequatly choosen so as to respect the periodicity of the lattices across the PBC. This operation may be challenging in most cases, but it is rather easy in the case of STGB as one of the box axis corresponds to the misorientation axis and guarantees the continuity of the two crystals in that direction. Here, we employ a strategy similar to the one in [7] to built the initial atomic structure of a GB. Ni interatomic interactions are described using a multibody semi-empirical potential proposed by Foiles and Hoyt [27], which is based on the so-called EAM formalism [28]. This potential is particularly well adapted to investigate mechanical and GB properties.

The initial arbitrary atomic configurations must be relaxed in order to find a possible ground state of the GB. This task may be challenging (see [5, 6] for example), here we employ a strategy similar to the 'gamma surface' calculations [8, 10, 29]. One grain is shifted with respect to the other grain, along the CSL basis vectors (contained in the GB plane). Atoms getting too close during this translation procedure are removed, then the system is relaxed using a classical conjugate gradient algorithm, and the GB energy of the corresponding relaxed GB structure is measured. This operation is done to obtain a fine map (typically $\approx 10^5$ points) of the GB energy as function of the the two translations directions, and the GB structure with the lowest energy is chosen as the most probable structure of

that particular GB. We compared the GB structures and energies obtained here to existing literature on similar GB [8, 10], and the agreement found allows to validate the approach to set our atomistic configurations.

Great attention must be paid to the dynamics simulation conditions used to study the GB migration [9, 10]. We employ the massively parallel MD code Lammps [30]. MD Simulations are conducted using the NVT ensemble. Starting from the relaxed 0K groundstate of the GB, the temperature in the system is progressively increased over 125 ps. The system is allowed to dynamically relax for another 125 ps. Then, the GB migration is triggered using the synthetic driving force proposed by Janssens et al. [31], which adds a force on atoms in the GB region. As a systematic study, the driving force is varied in the range $\approx$ [50-500MPa] and different temperature are considered [100-1000K]. Once again, our results on GB migration were confronted against existing data [9, 10] when available in order to validate the simulation conditions. More details can be found in [12]

### B. Phase Field model from Admal et al.

First, let us recall the Kobayashi-Warren-Carter PF model upon which the Admal et al. model is based. A 2D polycrystalline system $\Omega_0 \in \mathbb{R}^2$ is described with two scalar continuous fields $\theta(\mathbf{X})$ and $\phi(\mathbf{X})$, which represents the crystal orientation and the lattice order, respectively. The total free energy $W^{KWC}$ in the system is:

$$W^{KWC} = \int_{\Omega_0} \psi^{KWC} dV \tag{1}$$

with the free energy density functional expressed as:

$$\psi^{KWC} = \frac{\alpha^2}{2}|\nabla\phi|^2 + f(\phi) + g(\phi)s|\nabla\theta| + \frac{\epsilon^2}{2}|\nabla\theta|^2 \tag{2}$$

with,

$$f(\phi) = e(\phi - 1)^2 \tag{3}$$

$$g(\phi) = \phi^2 \tag{4}$$

The parameters $\alpha, \epsilon$ and $s$ are material constants. for non conservative order parameters, the time evolution of $\phi(\mathbf{X})$ and $\theta(\mathbf{X})$ are related to the partial derivative of $\psi^{KWC}$ with

respect to $\phi$ and $\theta$:

$$b^{\phi}\dot{\phi} = \alpha^2\Delta\phi - f_{,\phi} + g_{,\phi}s|\nabla\theta| \tag{5}$$

$$b^{\theta}\dot{\theta} = \mathrm{div}\left(\epsilon^2\nabla\theta + g_{,\phi}s\frac{\nabla\theta}{|\nabla\theta|}\right) \tag{6}$$

where $b^{\phi}$ and $b^{\theta}$ are inverse mobility functions for the two phase fields $\theta(\mathbf{X})$ and $\phi(\mathbf{X})$. The last equation is a singular diffusive equation due to the presence of the $\frac{\nabla\theta}{|\nabla\theta|}$ term. This is discussed at length in [18] and a non singular appoximation is also introduced, see [18] for more details. The term $g_{,\phi}s|\nabla\theta|$ tends to localized the interface, while the $\frac{\epsilon^2}{2}|\nabla\theta|^2$ tends to localize it. These two opposing effects act together to localize GB between grains and give a finite width to the interface [20].

Typically, the KWC model leads to grains where $\nabla\theta = 0$ and $\phi \approx 1$ (corresponding to a certain crystalline order) and localized GB, where $\nabla\theta \neq 0$ with $\theta$ smoothly transitioning from the orientation of the first grain into the orientation of the neighbouring grain and $\phi < 1$ (associated to disorder). This clear separation and definition of the grain and GB region $\in \Omega_0$ helped in providing an analytical solution of the KWC model [20].

To connect GB migration to potential mutual interaction with crystal dislocations, Admal and coworkers proposed to connect the KWC to a classical Crystal Plasticity framework [23]. A deformation map $\mathbf{y}(\mathbf{X},t)$ is associated to every material point $\mathbf{X}$ and time $t$. The deformation gradient $\mathbf{F}$ is thus:

$$\mathbf{F}(\mathbf{X},\mathbf{t}) = \nabla\mathbf{y} \tag{7}$$

To simulate large deformation, a multiplicative decomposition of the deformation gradient into an elastic $F^E$ and plastic contributions $F^P$ is assumed:

$$\mathbf{F} = \mathbf{F^E}\mathbf{F^P} \tag{8}$$

The lattice-invariant plastic distortion $F^P$ is associated to the plastic shear induced by dislocation slip. Different slip systems *alpha* are accounted in the model with distinct slip planes $\mathbf{s}^{\alpha}$ and directions $\mathbf{m}^{\alpha}$ and slip rates $v^{\alpha}$. The plastic distortion evolves as:

$$\dot{\mathbf{F}}^P = \mathbf{L^P}\mathbf{F^P} \tag{9}$$

$$\mathbf{L^P} = \sum_{\alpha=1}^{A} v^{\alpha}\mathbf{s}^{\alpha} \otimes \mathbf{m}^{\alpha} \tag{10}$$

with $L^P$ the plastic velocity gradient, and $\mathbf{s}^\alpha \otimes \mathbf{m}^\alpha$ the Schmid factor. In the model applied in 2D, four slip systems are available ($A$=4) having the following Burgers vectors:

$$\mathbf{s}^1 = (1, 0), \tag{11}$$

$$\mathbf{s}^2 = (0, 1), \tag{12}$$

$$\mathbf{s}^3 = \frac{1}{\sqrt{2}}(1, 1), \tag{13}$$

$$\mathbf{s}^4 = \frac{1}{\sqrt{2}}(-1, 1) \tag{14}$$

Finally, the Lagrangian strain is classically defined as:

$$\mathbb{E}^E = \frac{1}{2}\big((\mathbf{F^E})^\mathbf{T}\mathbf{F^E} - \mathbf{I}\big) \tag{15}$$

and will be appearing in the elastic free energy density. Next we introduce the connection between this CP framework and the KWC model.

From the seminal work from Read and Shockley [1], it has been long understood that lattice misorientation can be kinematically represented by an array of -discrete- dislocations. To connect to the KWC model and its diffuse picture of GB, the dislocation array has to be transformed into a continuous distribution [32] of Geometrically Necessary Dislocations (GND), that may be obtained from the plastic distortion:

$$\mathbf{G} = \mathbf{F^P}\ \mathrm{curl}\ \mathbf{F^P} \tag{16}$$

with the curl operator of a tensor field with respect to the materials coordinates. Crystal rotation in the model will be accommodated by the presence of a GND distribution, the following simplification is made: $\nabla\theta \approx |\mathbf{G}|$, and can be used to connect explicitly the CP framework and the KWC model. The total free energy density is thus:

$$\psi = \psi^b(\mathbb{E}^E, T) + \psi^{gb}(\phi, \nabla\phi, \mathbf{G}, T) \tag{17}$$

with $\psi^b(\mathbb{E}^E, T)$ the bulk free energy density mostly due to elastic distortions, and the free energy density associated to the GB, that derives from the KWC model as:

$$\psi^{gb} = \frac{\alpha^2}{2}|\nabla\phi|^2 + f(\phi) + g(\phi)s|\mathbf{G}| + \frac{\epsilon^2}{2}|\mathbf{G}|^2 \tag{18}$$

In this new framework, the kinematic variables are now : the displacement field $\mathbf{u} = \mathbf{y} - \mathbf{X}$, the shear rates $v^\alpha$ and the order parameter $\phi$. Conjugate forces associated to these variables, can be defined from a thermodynamically consistent approach. Interested readers

are referred to [23] for the full demonstration. We introduce a stress $\mathbf{P}$ conjugate of $\mathbf{F}$, a stress vector $\mathbf{p}$ conjugate of $\nabla\phi$ and a scale internal microscopic force $\pi$ power-conjugate of $\dot{\phi}$. Finally regarding the slip rates, we introduce an internal microscopic force $\Pi^\alpha$ power-conjugate of $v^\alpha$, and a microscopic stress $\xi^\alpha$ power conjugate of $\nabla v^\alpha$. The corresponding force balance equations and boundary conditions read: Macroscopic force balance:

$$\mathrm{Div}\mathbf{P} = \mathbf{0} \text{ in } \beta^0 \tag{19}$$

$$\mathbf{t} = \mathbf{P}\mathbf{N} \text{ on } \partial\beta^0 \tag{20}$$

Microscopic force balance for each slip system $\alpha$:

$$\mathrm{Div}\xi^\alpha - \Pi^\alpha = \mathbf{0} \text{ in } \beta^0 \tag{21}$$

$$\mathbf{\Xi}^\alpha = \xi^\alpha \cdot \mathbf{N} \text{ on } \partial\beta^0 \tag{22}$$

Microscopic force balance for $\phi$:

$$\mathrm{Div}\mathbf{p} - \pi = \mathbf{0} \text{ in } \beta^0 \tag{23}$$

$$s = \mathbf{p} \cdot \mathbf{N} \text{ on } \partial\beta^0 \tag{24}$$

These equations and boundary value conditions need to be solved numerically. Here, we reprise the resolution strategy and materials parameters employed in [23] and extend these results to more GB types in a systematic manner. For more details on the simulations conditions, see [23]. The initial geometry and kinematic variables are defined in figure 1.

## III. RESULTS

### A. GB structure

Figure 2 illustrates the atomic structure obtained after relaxation for some STGB, which consists of a succession of structural units that may or may not be connected to each others. In the latter case, an elastically distorted but defect free fcc lattice can be recovered and would correspond to well identifyable GB dislocatiion in LAGB. In the PF model, the GB structure is represented by the spatial distributions of the different GND tensor $\mathbf{G}$ components. At first, the GB is introduced with an initial $\theta$ field of the following form:

$$\tilde{\theta}(X_1) = -\frac{\theta_0}{2} + \frac{\theta_0}{1 + \exp\left(-2.5(X_1 - 10)\right)} \tag{25}$$

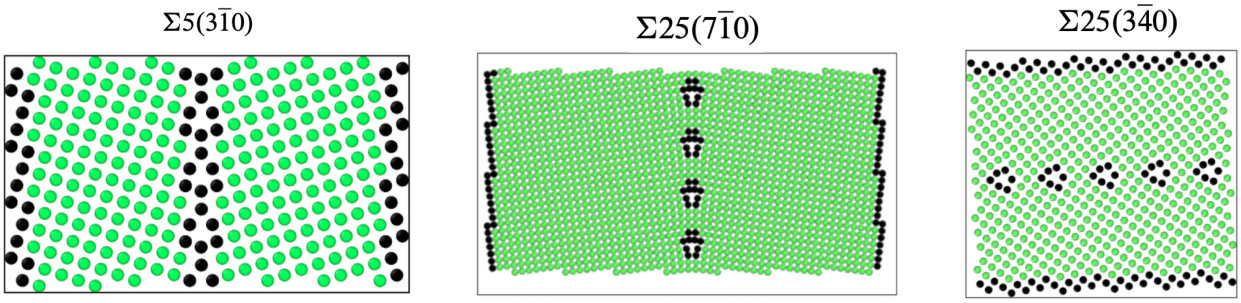


Figure 2. Atomic structures of a few CSL symmetric tilt grain boundaries relaxed using the Conjugate Gradient. Atoms in green correspond to those in close to perfect fcc lattice as described by a centrosymmetry parameter. Classically for these simulations, the GB structure correspond to a (periodic) succession or structural units of different geometry and periodicity. The two Σ25 GB exhibit well separated structural units, suggesting distinct and quantifiable GB dislocations.

Where $\theta_0$ is the misorientation angle of the GB. This expression for $\theta$ is however not an exact solution of the KWC equation (see at the end of the paper), and the fields will slightly relax from this arbitrary initial configuration. The model transforms this $\theta$ field into GND non-zero distributions in 2D:

$$G_{31} = -\cos(\tilde{\theta})\nabla\theta(x)$$
$$G_{32} = -\sin(\tilde{\theta})\nabla\theta(x)$$

Interestingly, both of the GND components $G_{31}$ and $G_{32}$ will be non-zero distributions in the model, as illustrated in figure 3. This contrasts with 'classical' kinematic picture of STGB devised by Read and Shockley, according to which STGB can be described only by a single set of edge dislocations, that would correspond to the sole $G_{31}$ component. However, in the PF the $G_{31}$ distribution is symmetrical while $G_{32}$ is antisymmetrical. The latter component thus does not contribute to the overall crystal rotation, nor to the elastic stresses (at least far from the GB). The figure 3 also shows the initial arbitrary $G_{ij}$ fields, and small changes can be seen from the comparison with the same fields after relaxation.

Figures 3.b and 3.c show the distributions of $G_{31}$ $G_{32}$ obtained after initial relaxation for all the considered STGB considered here. The $G_{ij}$ spatial distribution are similar for all GB, they however become larger and wider as the misorientation angle of the corresponding GB is large. The $G_{ij}$ spatial distributions thus seem to be rescaling of the same normalized distributions $\tilde{g}_{31}(x)$ and $\tilde{g}_{32}(x)$. This is confirmed in what follows.

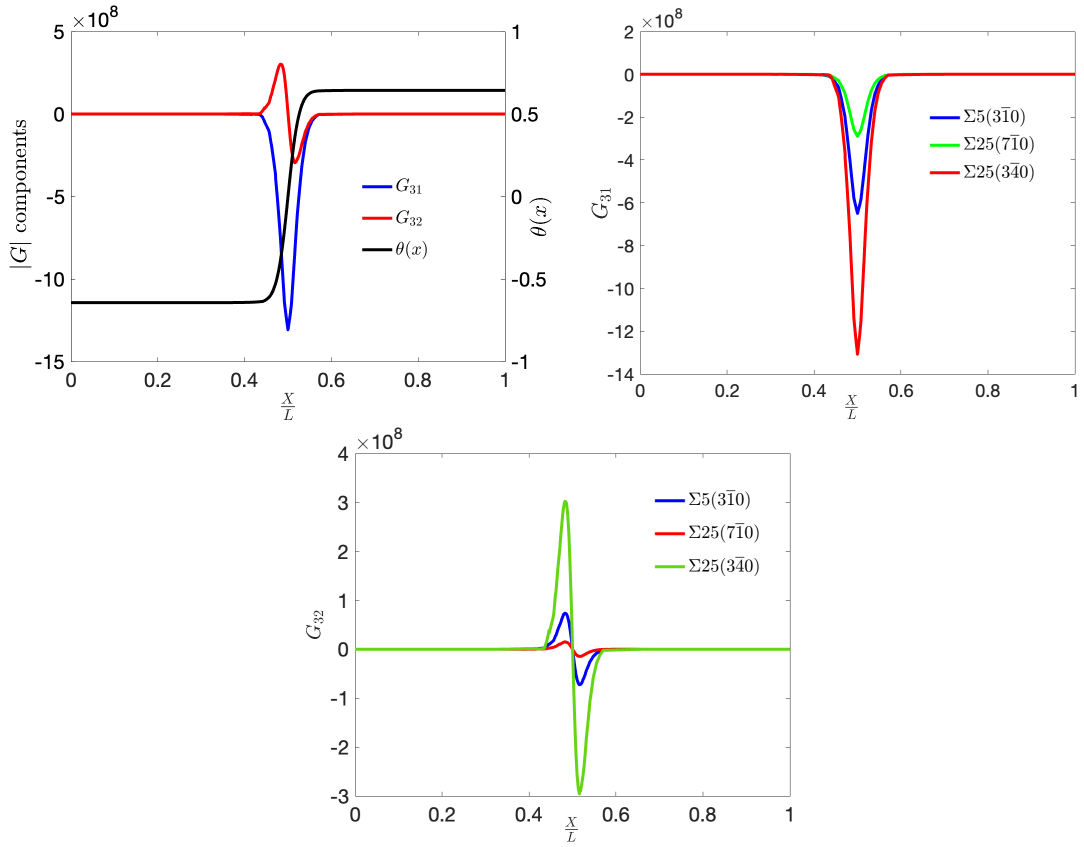


Figure 3. top left: Structure of $\Sigma25(3\bar{4}0)$ STGB in the Admal *et al.* PF model: Components of $|G|$ and the associated $\theta(x)$ field. Top right: Comparison of the $G_{31}$ distribution for three different STGB with increasing misorientation angle. Bottom: Comparison of the $G_{32}$ component for the same three different GBs.

Figure 4 displays the maximum value of the metric $|\mathbf{G}| = \sqrt{\mathbf{G} \cdot \mathbf{G}}$ as function of the misorientation angle and a nice linear increase can be seen. By dividing by the maximum value of the $\max(G_{ij})$ for every GB, rescaled distributions $\tilde{g}_{ij}(x)$ may be obtained and are shown in Figure 4. These rescaled distributions are virtually identical for the various considered STGB. This is an interesting feature of the Admal et al. PF model. For a single set of materials' parameters ($\alpha, \epsilon, e$ and $p$), all STGB are described by the same normalized spatial distributions $\tilde{g}_{ij}(x)$, and the scaling factor $\max(G_{ij})$, which depends upon the GB considered simply scaled with the misorientation angle. This feature may be exploited later for extrapolating results to other STGB or to propose simplified description of GB at the macroscale.

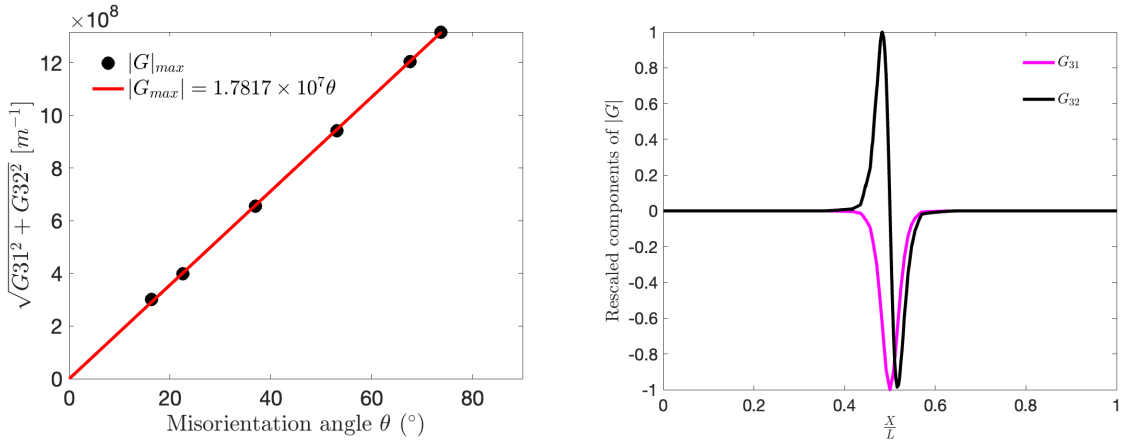


Figure 4. Left: $|G_{max}|$ versus $\theta$ (in degree) for all investigated grain boundaries. A clear linear trend is observed. When rescaling the $G_{31}$ and $G_{32}$ distributions of figure 3 by the corresponding $|G_{max}|$, all distributions for all the GB considered here collapse onto the same distribution $\tilde{g_{ij}}$ shown on the right.

### B. GB energy

Next, we compare the GB energy as obtained by the two proposed simulations. In the atomistic simulations the GB energy correspond to the excess energy resulting from the difference between the total potential energy $E_{with\,GB}$ of the simulation containing the GB and a volume without GB presence [1, 3]. Because the number of atoms $n_{at}$ may be changed during the procedure to find GB groundstate the GB energy is defined classically: $\gamma_{GB} = (E_{with\,GB} - n_{at} * E_{bulk})/S$ with $E_{bulk}$ the bulk energy of Ni atoms in perfect fcc structure. Since PF simulations are in 2D for now, while MD simulations were performed in 3D, the GB energy obtained in MD need to be converted in units of mJ/m by multiplying the raw GB energy by the GB dimension in MD simulations along the misorientation axis $y$, dimension that is absent in the PF simulations.

Figure 5 shows the GB energies (in units of J/m) as function of the misorientation angle for STGB. First, when considering MD data, the GB energy obtained here are in good agreement with other existing studies on these classical GB (with a maximum discrepancy of $\approx 20\%$ ). We can recall that the MD data was in nice agreement with other existing studies [8, 10, 11] In MD, it is well known that the GB energy is intimately controlled by the atomic structure of the GB and as a result these GB energy curves are non-convex functions

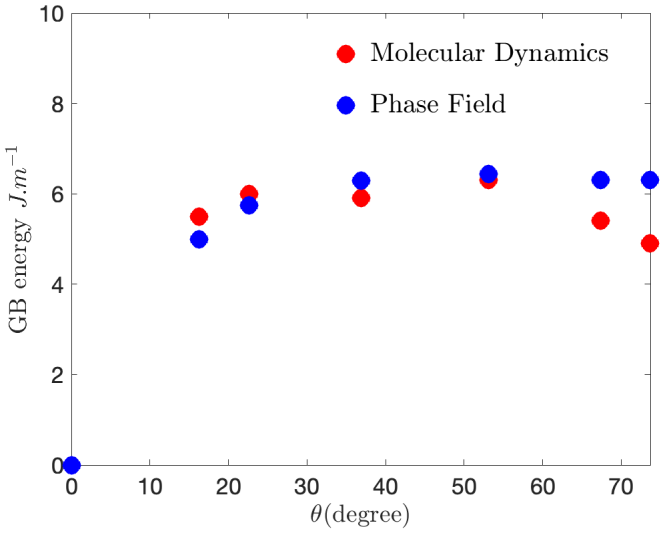


Figure 5. Comparison of the GB energy (in [J/m]) for the same STGB as calculated using MD and PF, as function of the misorientation angle. The GB energy from PF model increases monotically as function of the misorientation angle as expected from [23]

of misorientation angle and exhibit cusps at singular GB with local GB energy minima.

When now considering the PF data, the GB energy is now monotonous as was discussed before [23]. This is a consequence of the choice of function $g(\phi) = \phi^2(x)$ where a different choice could improve the agreement with the Read-Shockley model for the GB energy as function of misorientation angle [1]. The curve corresponding to PF data lacks the cusps in energy displayed on the MD curves, the quantitative values for the GB energy are however in a nice quantitative agreement with the MD values. This is a staggering results, as the PF has not yet been tweaked to particularly match this GB energy curve.

In the PF, it can be shown that the energy density is controlled by the $g(\phi)s|\mathbf{G}|+1/2\epsilon^2|\mathbf{G}|^2$ term to the first order. In the PF, the GB energy measured in PF scales with the metric $|\mathbf{G}|$. Recalling that $\mathbf{G} = \mathbf{F^P} curl \mathbf{F^P} = -\mathbf{F^e} curl \mathbf{F^e}$ we showed also earlier that $|\mathbf{G}|$ was increasing with the misorientation angle. The GB energy as described in PF is thus related to the elastic distortions induced by the GB presence. From a modelling standpoint, the GB energy can be decomposed into an elastic contribution far from the GB and a core contribution related to the distorted atomic arrangements seen at the GB. These contributions can be fully described by atomistics. However in the PF, only linear elasticity is included and multiplicative decomposition is employed. The elastic fields are continuous

across the GB, which would go through the core of the GB and where the lattice distortions seen in atomistics are typically non-linear. Therefore, and in a surprizing manner, linear elastic but continuous distortions are sufficient to predict -to the first order- the GB energy as described in atomistics simulations for the simple STGB considered here. This will be discussed further a bit later.

### C. GB migration and shear coupling

In a second set of simulations, we compare the dynamic property that is GB migration as described in atomistics and PF. In a recent study, we propose a systematic study of GB migration by MD in considering not only pure tilt but also pure twist and mixed GB for $\Sigma$ 5, 13 and 25 [12]. Here, we simply recall the main results and focus on the pure tilt GB. Migration of flat GB was triggered by using the methodology of the 'synthetic driving force' [31], that corresponds to adding a force per atom which derives from a potential energy favoring one grain. GB motion was measured while systematically varying the driving force-temperature $(P, T)$ parametric space. Figure 6 shows an example of a sequence of motion of a GB as described by MD. When the Driving Force (DF) is applied, the GB migrates and reach instantaneously a steady state. In this particular example, the GB migration is related to the nucleation and propagation of pairs of infinite disconnections (defects at the GB surface having both a dislocation and step character). The two disconnections propagate along the GB plane until their annihilation allowed by the PBC, making the GB flat again but translated when compared with the initial position. Since the disconnection Burgers vector $\mathbf{b_{disc}}$ has a non zero component along the in-plane $z$ direction, the so-called shear-coupling effect is observed according to which the normal GB motion is accompanied by a tangential motion.

In the PF, the GB migration is induced by applying a shear stress (through the shear coupling mechanism) and is associated to the translation of the center of GND distributions and $\theta$ field. Similarly to the atomistics, the GB motion reaches a steady state when the shear stress is applied. Figures 7 and 8 show illustrations of the migration as siimulated in the PF that is representative of other simulated GB. The application of an external load could have modified the GND distributions as it is the case in other continuous descriptions of GB, but here, the GND distributions are simple translations of the relaxed groundstate

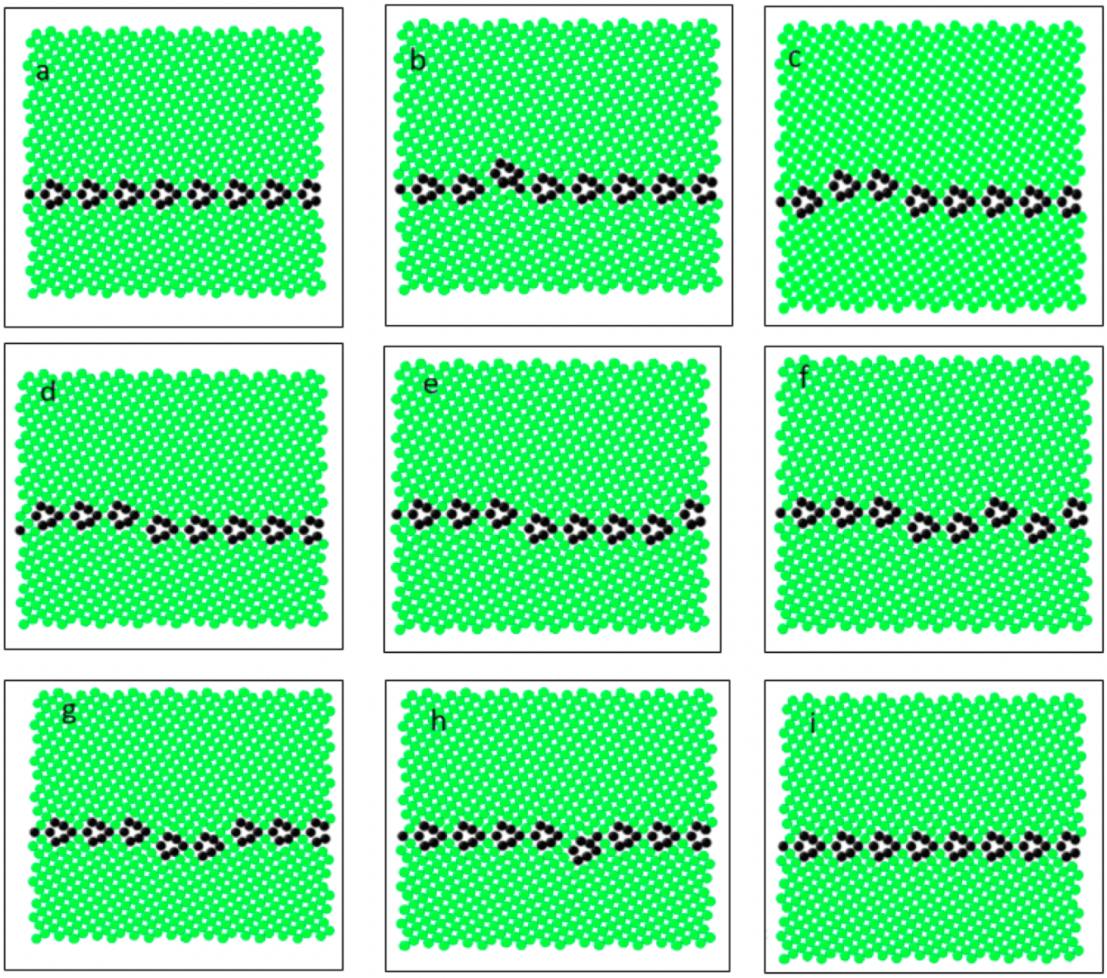


Figure 6. Sequence of motion of a $\Sigma13(2\bar{3}0)$ tilt grain boundary. From its Initial relaxed structure a), this GB migration is mediated by b) nucleation and c) to i) propagation of pairs of disconnections. Atoms are coloured by CNA with green atoms are close to the perfect FCC positions and black atoms belong to defects.

GND distributions (see figure 7.b). From a mechanistic standpoint, this is what should be desired, as the GB structures should not be affected by the application of a external stress (this is true for relatively small stresses, but large stresses may induce GB structural changes [33, 34]). From a PF theoretical standpoint, this means that the microscopic force balance is mostly preserve during migration.

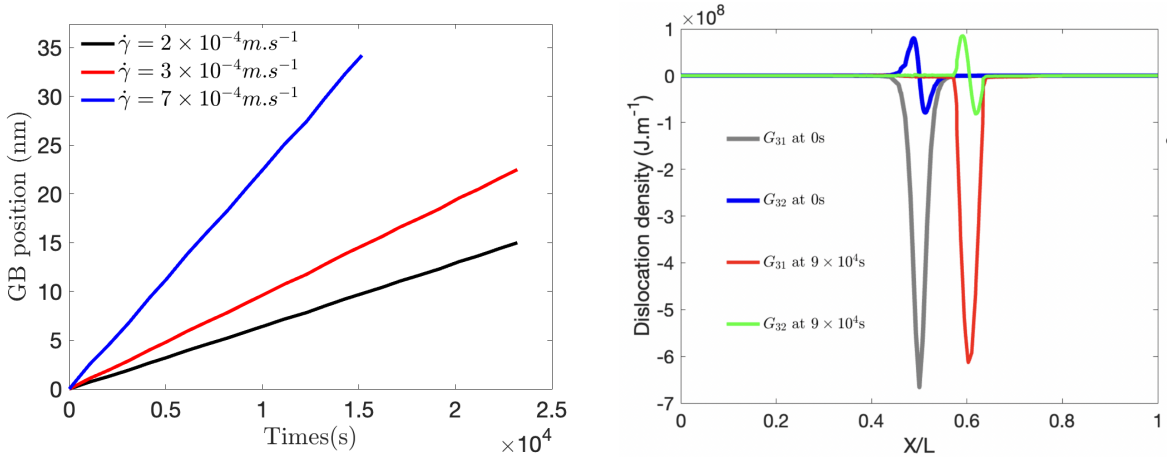


Figure 7. Left: Position of the $\Sigma 25(7\bar{1}0)$ STGB as function of time for different shear rate ($\dot{\gamma}$) during a migration simulation in PF. Right: Evolution of the $G_{31}$ and $G_{32}$ distributions at different time steps during the motion of $\Sigma 5(3\bar{1}0)$ grain boundary at a shear rate of $\dot{\gamma} = 8 \times 10^{-4} ms^{-1}$.

### D. GB migration velocity

Among the 25 GB considered in MD [12], three different types of migration behaviour were unambiguously observed as function of the temperature impact of the motion, in agreement with existing MD studies [9, 10]. When focusing on the STGB, two of the three of these migration behaviours were observed and are illustrated in Figure 9. A low driving force and low temperature, some GB exhibit a non-linear velocity as function of driving force and the velocity increases with the temperature. This first behaviour is typical of the classical thermally-activated picture of GB migration. The values of velocity observed here are in qualitative agreement with existing studies performed in similar conditions, when available [9, 10, 13]. Interestingly, a linear regime is observed at larger driving force as the applied mechanical work is sufficient to overcome the activation barrier. This type of transition from thermally activated to (non-viscous) linear regime was also observed for the motion of dislocations in bcc Fe [35, 36]. In [12], the MD data allowed to formulate a phenomenological mesoscopic velocity law as:

$$v_{MD}(GB, P, T) = A * P \exp\left(-\frac{\Delta H(P,T)}{k_B T}\right)$$

where $\Delta H(P,T)$ is the activation enthalpy associated to the GB migration, and is a function of both $P, T$. Some other GB exhibit a linear relationship between the migration velocity

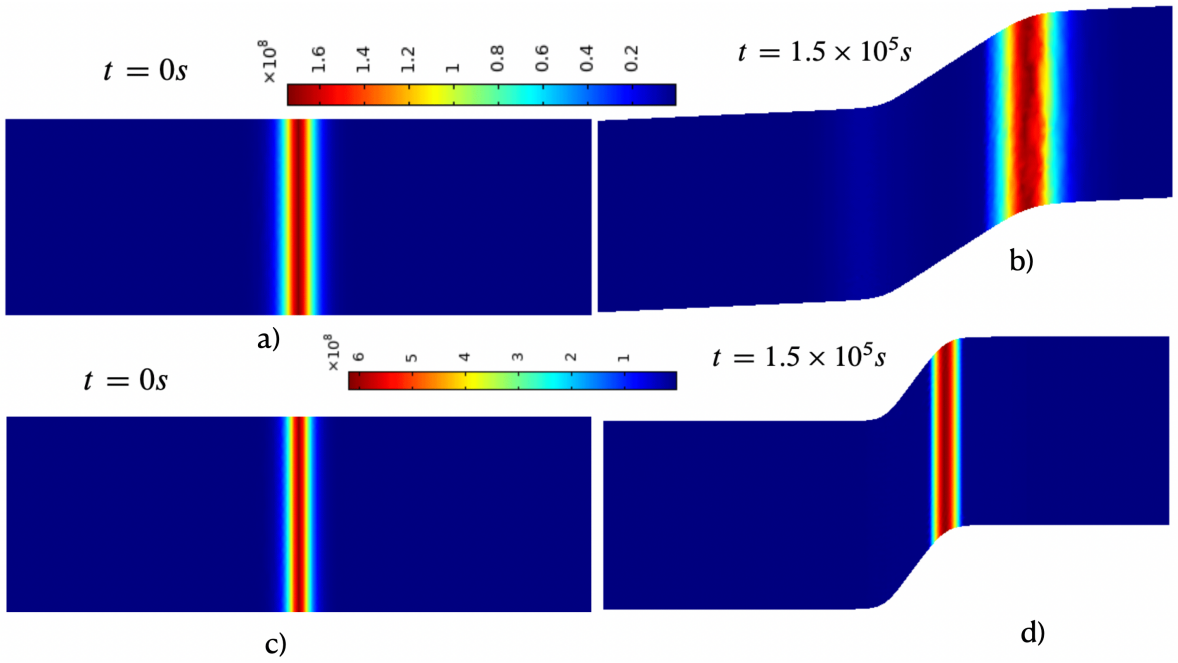


Figure 8. Illustration of the GB migration in PF through the evolution of the metric $|G|$ in a)$\Sigma 25(7\bar{1}0)$, c) $\Sigma 5(3\bar{1}0)$ initial and b) $\Sigma 25(7\bar{1}0)$, d) $\Sigma 5(3\bar{1}0)$ deformed configuration at shear rate $\dot{\gamma} = 2 \times 10^{-4} ms^{-1}$.

and the driving force as shown in figure 9. The slope $B(T)$ decreases with temperature, suggesting a phonon dragging mechanism. The velocity law for this kind of dynamic behaviour is:

$$v_{MD}(GB, P, T) = B(T)P$$

This type of migration is often observed for GB that can be clearly identified as subgrain boundary with clearly separated GB dislocations. However, predicting the type of GB migration from the macroscopic degrees of freedom for GB or even when the GB atomic structure is known is still a key challenge in the field.

We apply the same systematic exploration of the P-T parametric space to our PF simulations of the GB migration. These results are shown in Figure 10. Interestingly, the PF recovers qualitatively the different velocity behaviour observed in MD. For example the $\Sigma$ 5 exhibits a non linear increase of the migration velocity with the applied shear. This velocity also increases when the temperature is increased. This type of behaviour would be consistent with the thermally activated behaviour observed for the same GB in atomistics. The velocities values are however not on par with the MD data, as the inverse mobility function

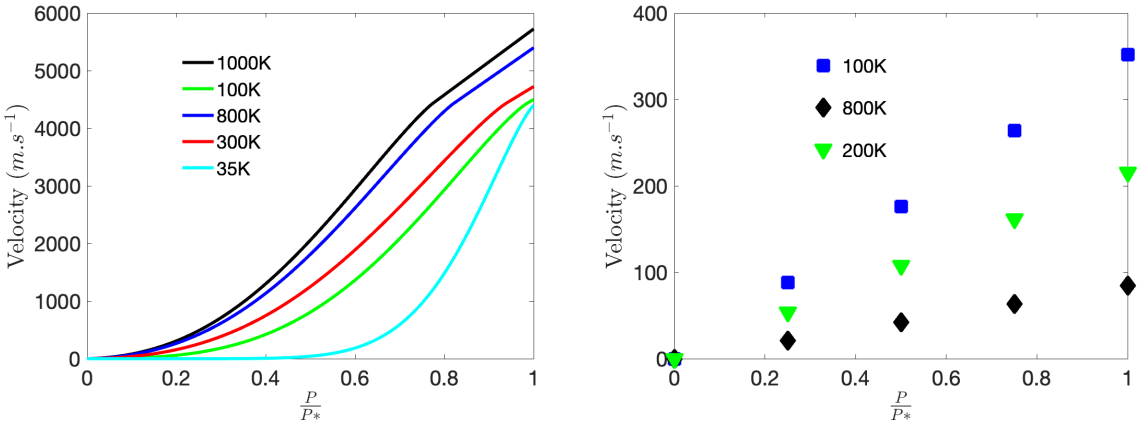


Figure 9. Two of the GB migration types obtained by MD [12]. Left: Prediction of the velocity function given in the text for the thermally-activated migration of $\Sigma5(3\bar{1}0)$ at different temperature and driving force. Right: linear velocity dependence with $P$ for a $\Sigma25(3\bar{4}0)$ at different temperature and driving force

$b_\phi$ $b_\theta$ were choosen arbitrarily for now [23]. Some other grains, like the $\Sigma$ 25, exhibit a different behaviour with a linear increase of velocity with the applied shear and the linear slope decreases when temperature increases. This behaviour would be in agreement with the viscous type behaviour observed for the same GB in MD.

In MD, the different mobility are typically explained by the difference in atomic structure, while no prediction is still available. Since the PF has no explicit description of the GB core, the difference in velocity dependence upon temperature for the different GB must find a different explanation. We have shown also that all the STGB are described by identical GND distributions scaled by a factor $\max(|G|)$. This cannot explain these differences. However, when migrating, the same GND description can involve different slip systems out of the four slip systems available in the 2D PF, and the resulting interaction and kinetics between these slip systems may explain the difference. This should be investigated further.

## IV. DISCUSSION

In this discussion, we are going to address two main points. The first one is an attempt to explain the surprizing qualitative agreement of PF with the reference data form MD, and the second point is how to reach a quantitative agreement between the two approaches.

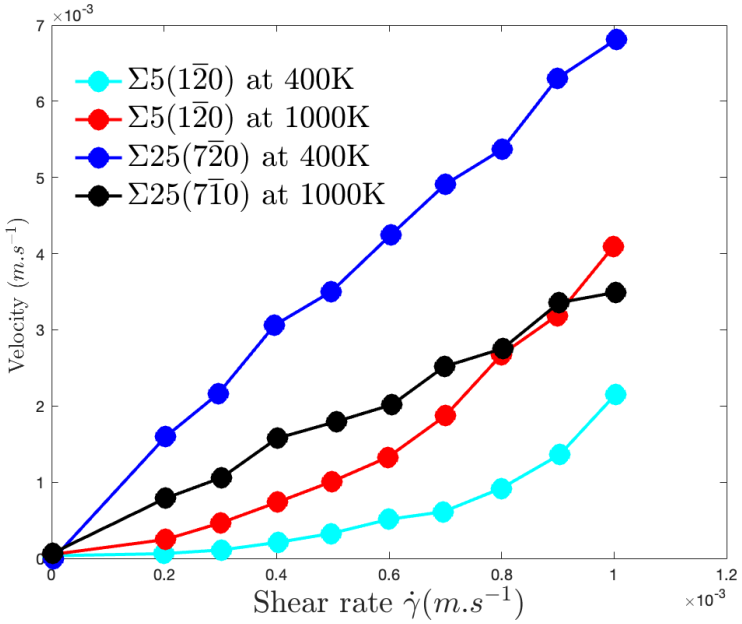


Figure 10. Comparison of migration velocity simulated in the PF between $\Sigma25(7\bar{1}0)$ and $\Sigma5(1\bar{2}0)$ at different temperatures and shear rates

### A. On the rather good agreement between MD and PF

The nice agreement between PF and MD, which is qualitative on most of the features considered here, may appear surprizing at first as the PF was not set up initially to match the MD results especially for large angle GB like some of the ones considered here. First, the PF materials parameters $(\alpha, \epsilon, p, e)$, while not chosen to reproduce the MD results for now, exhibit values close to the ones suggested in [19] where they were scaled with respect to a typical latent heat value for metals. This lead to proper dimensions of the GB thickness of the order of nm. The elastic properties correspond to the classical isotropic approximations for Ni.

This being said, the GB energy in particular is commonly though to be mostly controlled by large distortion associated to the atomic arrangements at the core of GB. In the PF, GB are simply described by GND distributions coming from elastic (respectively plastic) distortions. The elastic gradient is thus continuous across the GB, including at the GB core. The elastic and plastic component of the deformation gradient are however obtained from a multiplicative decomposition, that works well for large distortions. The PF was able to reproduce the MD data at the exception of the cusps typical of singular GB. This simple

modelling of GB as continuous GND distribution appears thus to be sufficient for STGB, even for LAGB, but not singular GB.

The qualitative agreement between PF and MD is also surprizing when now considering the migration of GB. At the atomistic scale, the GB migration has to be related to the atomic structure of the GB, even if the full understanding is still out of reach. The atomic structure may control the choice and features of the elementary mechanisms involved in the GB migration, and consequently, the associated kinetics. There is a debate in the literature as to whether the GB mobility is an intrinsic mobility of GB as defects at GB may then activate other migration modes. Here, the PF can not explicitly reproduce these effects, but the nice qualitative agreement must be explained in another way. We suggested here, that the selection of slip systems, their interactions and the certainly the associated dissipated energy control the velocity dependence of GB migration upon temperature. These general effects could as well be effective in atomistic simulations and thus could contribute to explain the observed GB kinetics.

### B. Towards more quantitative PF simulations

Our existing MD results provide GB energies and complex mobility functions for about 25 different CSL grain boundaries with a [001] misorientation axis. While the two types of simulations are capable of describing similar mechanisms, connecting the two approaches is not straightforward. In particular, phase field relies upon continuous fields, whose direct determination from atomistic calculations seems unclear (this is particularly true for the order parameter $\Phi(\mathbf{x})$ and the generalized forces). In the original form, parametrizing a KWC model with MD, would require to run many PF simulations and a lot of trials and errors in an attempt to find the correct set of PF material parameters to match the GB energy and mobility from MD. In addition to be extremely costly, there is no guaranty that this procedure will converge to a unique set of PF material parameters identified this way.

The objective of this final section is to present a way to parameterize the so-called Kobayachi-Warren-Carter Phase Field (PF) model using atomistic data obtained from Molecular Dynamics (MD), to describe the Grain Boundary migration in polycrystals. Here, we derive a semi-analytical solution of the phase field set of equations of the 1D problem of a single GB in a bicrystal under static and steady motion conditions.

We start recalling the KWC model. The energy density can be written:

$$\psi^{KWC} = \frac{\alpha^2}{2}|\nabla\phi|^2 + f(\phi) + g(\phi)s|\nabla\theta| + \frac{\epsilon^2}{2}|\nabla\theta|^2 \tag{26}$$

with,

$$f(\phi) = e(\phi - 1)^2 \tag{27}$$

$$g(\phi) = \phi^2 \tag{28}$$

The parameters $\alpha, \epsilon$ and $s$ are material constants. for non conservative phase fields, the time evolution of $\phi(\mathbf{X})$ and $\theta(\mathbf{X})$ are related to the partial derivative of $\psi^{KWC}$ with respect to $\phi$ and $\theta$:

$$b^{\phi}\dot{\phi} = \alpha^2\Delta\phi - f_{,\phi} + g_{,\phi}s|\nabla\theta| \tag{29}$$

$$b^{\theta}\dot{\theta} = \text{div}\left(\epsilon^2\nabla\theta + g_{,\phi}s\frac{\nabla\theta}{|\nabla\theta|}\right) \tag{30}$$

It must be noted that the formulation above, which includes the term $\nabla\theta/|\nabla\theta|$ leads to a singular diffusive equation. A non-singular approximation may be found in [18], but this did not seemed to be required in the 1D solution proposed in what follows.

### *1. Analytical solution for the bicrystal*

Here, we reprise the analysis proposed in [20, 23] that relies on a formal asymptotic expansion of the model. Since the model tends to localize grain boundaries, the solution is typically separated onto two domains. In the region corresponding to the grain interior, $\nabla\theta = 0$. The boundary conditions are:

$$\phi(\pm L) = 1,\ \theta(\pm L) = \pm\theta_0/2 \tag{31}$$

Where the coordinate $x$ is delimited by $\pm L$. A grain boundary exists at the origin and is bounded by $\pm\xi_0$, where $\nabla\theta \neq 0$. the fields $\phi$ and $\theta$ are symmetric and anti-symmetric about the origin, respectively. Under the static condition and outside of the GB, Eq. 4 becomes:

$$\alpha^2\Delta\phi - f_{,\phi} = 0 \tag{32}$$

$$\frac{\alpha^2}{2}\phi_{,\phi} - f(\phi) = c \tag{33}$$

where $c$ is an integration constant. Integrating the previous equation leads to:

$$L - x = \int_{\phi}^{1} \frac{\alpha}{\sqrt{2(f(\tilde{\phi}) + c)}} d\tilde{\phi} \tag{34}$$

In order to obtain a closed form analytical solution for $\phi(x)$, one has to find an analytical function for the integral in the rhs of the previous equation, and then one has to be able to invert that function. Luckyly, this is the case for the choice of $f(\phi)$ in Eq. 3. The solution outside the GB is thus:

$$\phi(x) = 1 - \sqrt{\frac{c}{e} \frac{\tanh^2(\lambda(x))}{1 - \tanh^2(\lambda(x))}} \tag{35}$$

$$\lambda(x) = \frac{\sqrt{2e}}{\alpha}(x - L) \tag{36}$$

$$c = \left( \frac{1 - tanh^2(\lambda(\xi_0))}{tanh^2(\lambda(\xi_0))} \right) f(\phi_2) \tag{37}$$

In the GB region and still in the static case, $\nabla\theta \neq 0$, $\phi(x)$ and $\theta(x)$ must respect the system of PDE:

$$\alpha^2 \Delta\phi - f_{,\phi} + g_{,\phi} s |\nabla\theta| = 0 \tag{38}$$

$$\left(\epsilon^2 \nabla\theta + g_{,\phi} s\right)_{,x} = 0 \tag{39}$$

From Eq. 12, one can deduce that $\epsilon^2 \nabla\theta + g_{,\phi} s = cste.$ and the BC reads $\phi_{,x} = 0$ at $x = \xi_0$, thus:

$$\theta_{,x} = \frac{s}{\epsilon^2}(g(\phi_2) - g(\phi)) \tag{40}$$

Inserting the last equation into Eq. 12 yields:

$$\left( \frac{\alpha^2}{2} \phi_{,x} - f(\phi) + \frac{s^2}{2\epsilon^2}(g(\phi_2) - g(\phi))^2 \right)_{,x} = 0 \tag{41}$$

using the BC, $\alpha^2/2(\phi_{,x})^2 - f(\phi_2) = c$, thus:

$$\frac{\alpha^2}{2} \phi_{,x} - f\phi + \frac{s^2}{2\epsilon^2}(g(\phi_2) - g(\phi))^2 = c \tag{42}$$

Integrating previous equation may provide an equation in the form of an integral to find $\phi$:

$$x(\phi) = \int_{\phi_1}^{\phi} \frac{\alpha}{\sqrt{2(f(\tilde{\phi}) + c) - \frac{s^2}{\epsilon^2}(g(\phi_2) - g(\phi))^2}} d\tilde{\phi} \tag{43}$$

Similarly to Eq. 9 outside the GB domain, one has to find an analytical and inversible solution to the rhs of this equation in order to dispose of a closed form expression. However,

the addition of the $(g(\phi_2)-g(\phi))^2$ makes it harder to solve. The integral Eq. 16 can also be presented in as a ODE. Under this form, the main difficulty, now evident, is that this ODE is a non-linear 1st order ODE.

$$\frac{d\tilde{\phi}}{dx} = \frac{1}{\alpha}\sqrt{2(f(\tilde{\phi})+c) - \frac{s^2}{\epsilon^2}(g(\phi_2)-g(\phi))^2} \tag{44}$$

We tried to solve this ODE using Laplace Transforms (LT) without success, this is certainly due to the presence of terms in power of $\phi^4$ and $\phi^2$ in the polynomial $P(\phi)$ under the square root, for which there is no known LT.

Alternatively, we consider tables of known integrals, whose form would be similar to the form of Eq. 16. To do this, the polynomial $P(\phi)$ must first be reworked.

$$P(\phi) = -\frac{s^2}{\epsilon^2}\phi^4 + (2\frac{s^2}{\epsilon^2}\phi_2^2+1)\phi^2 - 2\phi + (2c+1-\frac{s^2}{\epsilon^2}\phi_2^4) \tag{45}$$

$$= \frac{s^2}{\epsilon^2}\left(-\phi^4 + (2\phi_2^2+\frac{\epsilon^2}{s^2})\phi^2 - 2\frac{\epsilon^2}{s^2}\phi + \frac{\epsilon^2}{s^2}(2c+1-\frac{s^2}{\epsilon^2}\phi_2^4)\right) \tag{46}$$

$$= \frac{s^2}{\epsilon^2}\left(-(\phi-r_1)(\phi-r_2)(\phi-r_3)(\phi-r_4)\right) \tag{47}$$

Where $r_i$ are roots of the polynomial Eq. 19. The roots of this quartic equations can still be analytically obtained using Ferrari's solution.

### *2. $P(\phi)$ admits three distinct roots*

Assuming the root $r_3$ must be double. One can thus find an analytical solution for the integral Eq. 17:

$$x(\phi) = \frac{\alpha\epsilon}{s}\int_{\phi_1}^{\phi} \frac{1}{\sqrt{-(\tilde{\phi}-r_1)(\tilde{\phi}-r_2)(\tilde{\phi}-r_3)^2}} d\tilde{\phi} \tag{48}$$

$$c_1 + x = \frac{\alpha\epsilon}{s}\left[\frac{2}{\sqrt{r1-r3}\sqrt{r3-r2}}\tan^{-1}\left(\frac{\sqrt{r3-r2}\sqrt{r1-\tilde{\phi}}}{\sqrt{r1-r3}\sqrt{r2-\tilde{\phi}}}\right)\right]_{\phi_1}^{\phi} \tag{49}$$

The function is also inversible, leading to the solution for $\phi(x)$:

$$\phi(x) = \frac{r_1 A - r_2 \tanh^2\left(B(c_2-x)\right)}{A - \tanh^2\left(B(c_2-x)\right)} \tag{50}$$

$$A = \frac{r_3-r_2}{r_1-r_3} \tag{51}$$

$$B = \frac{s\sqrt{(r_1-r_3)(r_3-r_2)}}{2\alpha\epsilon} \tag{52}$$

where the periodic tan function has been replaced by a non-periodic tanh function. A new integration constant $c_2$ is introduced $c_2 = c_1 - \frac{\alpha\epsilon}{s}G(\phi_1)$, with $G(\phi)$ is the primitive on the rhs of equation 22. It can be checked that this expression of $\phi(x)$ is a solution by inserting it into equations 16 or 17.

the solution for $\theta(x)$ can be obtained from integration of:

$$\theta_{,x} = \frac{s}{\epsilon^2}(\phi_2^2 - \phi^2(x)) \tag{53}$$

$$\theta(x) = \frac{s}{\epsilon^2}\phi_2^2 x + \frac{s}{\epsilon^2}\frac{1}{2(A-1)^2 B}\Big[C\tanh^{-1}\left(\frac{\tanh(Bx)}{\sqrt{A}}\right) \tag{54}$$

$$\frac{D\tanh(Bx)}{A-\tanh^2(Bx))} - EBx\Big] \tag{55}$$

$$C = \sqrt{A}\left(A(3r_1+r_2)(r_1-r_2) + (3r_2+r_1)(r_2-r_1)\right) \tag{56}$$

$$D = A(A-1)(r_1-r_2)^2 \tag{57}$$

$$E = 2(r_2 - Ar_1)^2 \tag{58}$$

The integration constant may be implicitly defined as:

$$c = -f(\phi_1) + \frac{s^2}{2\epsilon^2}(g(\phi_2) - g(\phi_1))^2 \tag{59}$$

which is problematic as the solution for $\phi$ depends on its own extremas.

Finally, it can be checked that the two solutions for $\phi(x)$ and $\theta(x)$ can be analytically integrated to calculate the GB energy and the GB mobility.

### *3. $P(\phi)$ admits four distinct roots*

In the most general case, the polynomial $p(\phi)$ admits four different roots. The solution can still be obtained but in a semi-analytical manner only as it implies an incomplete Elliptic integral of the first kind $F(x|m)$.

$$x(\phi) = \frac{\alpha\epsilon}{s}\int_{\phi_1}^{\phi}\frac{1}{\sqrt{-(\tilde{\phi}-r_1)(\tilde{\phi}-r_2)(\tilde{\phi}-r_3)(\tilde{\phi}-r_4)}}d\tilde{\phi} \tag{60}$$

$$c_1 + x = \frac{\alpha\epsilon}{s}\left[\frac{2}{\sqrt{r1-r3}\sqrt{r2-r4}}\mathrm{F}\left(\sin^{-1}\left(A\sqrt{\frac{r1-\tilde{\phi}}{r2-\tilde{\phi}}}\right)\Big|m\right)\right]_{\phi_1}^{\phi} \tag{61}$$

$$A = \sqrt{\frac{r2-r4}{r1-r4}} \tag{62}$$

$$m = \frac{(r_2-r_3)(r_1-r_4)}{(r_1-r_3)(r_2-r_4)} \tag{63}$$

Elliptic integral of the first kind is defined as $F(x|k) = \int_0^x \frac{dy}{\sqrt{1-k^2\sin^2 y}}$, with the elliptic modulus $k$ that must satisfy $0 < k < 1$. The Jacobi Amplitude $am(x,k)$ is defined as the inverse of the elliptical integral F: $am(F(x,k),k) = x$. We can also introduce one of the Jacobi Elliptic function $sin(x,k) = sin(am(x,k))$. All these functions can be numerically evaluated by various procedures [NIST Digital Library of Mathematical Functions. Ch. 19].

$$\phi(x) = \frac{r_2 \mathrm{sn}^2(\lambda,k) - r_1 A^2}{\mathrm{sn}^2(\lambda,k) - A^2} \tag{64}$$

$$\lambda = \frac{s}{\alpha\epsilon}\frac{\sqrt{(r_1-r_3)(r_2-r_4)}}{2}(c_1 - x) + G(\phi_1) \tag{65}$$

With, $G(\phi_1)$ is the primitive function appearing on the rhs of eq. 34. While, the expression for $\phi(x)$ is rather short and simple, this is not the case anymore for $\theta$ field and the GB energy. A semi-analytical expression cans still be obtained for these two terms thanks to Mathematica and exhibit a long sum of various Elliptic functions and integrals. For the sake of conciseness however, and as $\phi$ is well bounded between $\phi_1$ and 1, approximating $\phi$ using a Taylor Series on different domains of $\phi$.

The advantage of this explicit expression is that now the two remaining unknowns $\phi_1$ and $\phi_2$ can be obtained from very robust Newton-Raphson scheme to solve the following non-linear equations:

$$c = -f(\phi_1) + \frac{s^2}{2\epsilon^2}(g(\phi_2) - g(\phi_1))^2 \tag{66}$$

$$\theta_0 = \frac{\alpha s}{\epsilon^2}\int_{\phi_1}^{\phi_2} \frac{g(\phi_2) - g(\phi)}{\sqrt{2(f(\tilde{\phi}) + c) - \frac{s^2}{\epsilon^2}(g(\phi_2) - g(\phi))^2}} d\tilde{\phi} \tag{67}$$

$$Ł = \int_{\phi_1}^{\phi_2} \frac{\alpha}{\sqrt{2(f(\tilde{\phi}) + c) - \frac{s^2}{\epsilon^2}(g(\phi_2) - g(\phi))^2}} d\tilde{\phi} + \int_{\phi_2}^{1} \frac{\alpha}{\sqrt{2(f(\tilde{\phi}) + c)}} d\tilde{\phi} \tag{68}$$

The Jacobian appearing in the Newton-Raphson algorythm for this multi-variable problem is calculated analytically from mathematica.

A direct comparison with numerical calculations of the KWC model presented in [23] is possible. The following materials parameters were used:

$$\alpha^2 = 5.3 \times 10^{-9} \tag{69}$$

$$\epsilon^2 = 2.1333 \times 10^{-10} \tag{70}$$

$$e = 2.1 \times 10^9 \tag{71}$$

$$s = 0.17 \tag{72}$$

Interestingly $s$ has to be greatly reduced compared to the value used in the numerical solution as the analytical model does not smooth out the $\nabla\theta$ in the GB region. The comparison is shown in figure 11. In the analytical model, $\phi_1 = 0.875$, $\phi_2 = 0.9$ and $\xi_0 = 0.7$ nm.

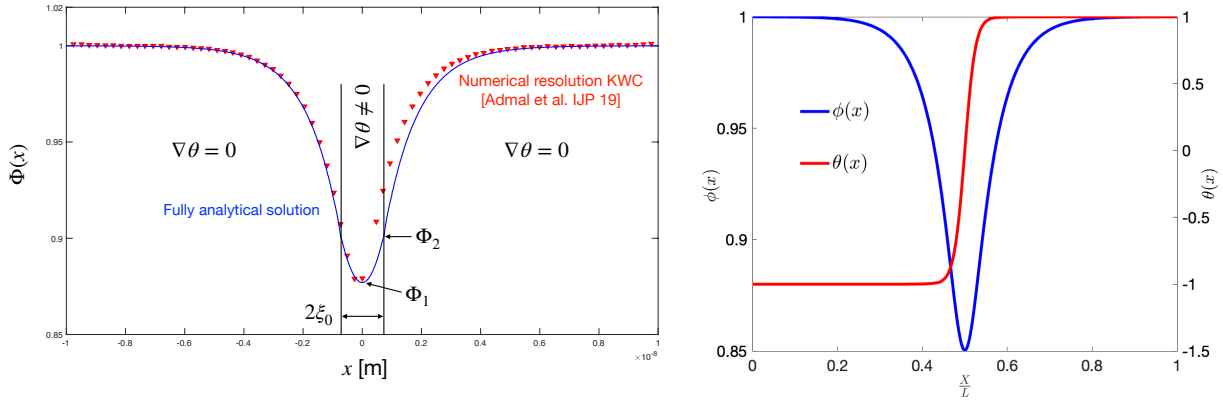


Figure 11. Left: Validation of the analytical (1D) model with the numerical resolution of the (2D) KWC model from [23]. Right: Analytical solutions for both $\theta$ and $\phi$ fields for $\Sigma5(3\bar{1}0)$.

Finally, the link with Admal et al. PF model can be recovered, recalling that $|\mathbf{G}| = \nabla\theta(x)$, the components of $|\mathbf{G}|$ are thus recovered, and are shown in Figure z.

$$G_{31} = -\cos(\tilde{\theta})\nabla\theta(x)$$
$$G_{32} = -\sin(\tilde{\theta})\nabla\theta(x)$$

*4. Mesoscale properties of the GB*

Finally, going back to [20], the mescoscale properties of a GB *i.e.* GB energy $v$ and mobility $M$ can be expressed from the $\phi$ and $\theta$ fields.

$$\gamma = s\Delta\theta_0\phi_2^2 + 2\alpha\int_{\phi_{max}}^{1}\sqrt{2(f(\tilde{\phi})+c)}\,d\tilde{\phi} \tag{73}$$

$$+2\alpha\int_{\phi_{min}}^{\phi_{max}}\sqrt{2(f(\tilde{\phi})+c) - \frac{s^2}{\epsilon^2}(g(\phi_2)-g(\phi))^2}\,d\tilde{\phi} \tag{74}$$

$$M^{-1} = \int_{-L}^{L}\left(b^{\phi}\phi_{,x}^2 + b^{\theta}\theta_{,x}^2\right)dx \tag{75}$$

with $b^{\phi}$ and $b^{\theta}$ inverse mobility functions associated to the time variation of $\phi$ and $\theta$, respectively. The velocity of the GB is $v = M\kappa\gamma$ and is the results of capillarity trough $\gamma$ and curvature driving forces through curvature $\kappa$. In the present 1D model, the curvature $\kappa$ is

undefined. We may expert that the mobility will be preserved when the GB migrates under other driving forces.

**ACKNOWLEDGEMENTS**

The authors would like to thank N. Admal, A. Ask, S. Forest, J. Marian, U. Salman and V. Taupin for valuable comments and stimulating discussions regarding this work.

**REFERENCES**

[1] A. P. Sutton and R. W. Balluffi. *Interfaces in crystalline materials*. Clarendon Press, 1995.

[2] Gunter Gottstein and Lasar S. Shvindlerman. *Grain Boundary Migration in Metals: Thermodynamics, Kinetics, Applications*. CRC Press, June 1999.

[3] Y. Mishin, M. Asta, and Ju Li. Atomistic modeling of interfaces and their impact on microstructure and properties. *Acta Materialia*, 58(4):1117–1151, February 2010.

[4] Jian Han, Spencer L. Thomas, and David J. Srolovitz. Grain-boundary kinetics: A unified approach. *Progress in Materials Science*, 98:386–476, October 2018.

[5] T. Frolov and Y. Mishin. Thermodynamics of coherent interfaces under mechanical stresses. II. Application to atomistic simulation of grain boundaries. *Physical Review B*, 85(22), June 2012.

[6] Timofey Frolov, David L. Olmsted, Mark Asta, and Yuri Mishin. Structural phase transformations in metallic grain boundaries. *Nature Communications*, 4:1899, May 2013.

[7] Arash D. Banadaki and Srikanth Patala. An efficient algorithm for computing the primitive bases of a general lattice plane. *Journal of Applied Crystallography*, 48(2):585–588, April 2015.

[8] David L. Olmsted, Stephen M. Foiles, and Elizabeth A. Holm. Survey of computed grain boundary properties in face-centered cubic metals: I. Grain boundary energy. *Acta Materialia*, 57(13):3694–3703, August 2009.

[9] David L. Olmsted, Elizabeth A. Holm, and Stephen M. Foiles. Survey of computed grain boundary properties in face-centered cubic metals—II: Grain boundary mobility. *Acta Materialia*, 57(13):3704–3713, August 2009.

[10] Eric R. Homer, Srikanth Patala, and Jonathan L. Priedeman. Grain Boundary Plane Orientation Fundamental Zones and Structure-Property Relationships. *Scientific Reports*, 5(1), December 2015.

[11] Vasily V. Bulatov, Bryan W. Reed, and Mukul Kumar. Grain boundary energy function for fcc metals. *Acta Materialia*, 65:161–175, February 2014.

[12] Etienne Ngenzi, Zakaria El Omari, Brigitte Bacroix, and Sylvain Queyreau. Mobility functions for [001] CSL grain boundaries in Ni from molecular dynamics. December 2021.

[13] Chuang Deng and Christopher A. Schuh. Diffusive-to-ballistic transition in grain boundary motion studied by atomistic simulations. *Physical Review B*, 84(21):214102, December 2011.

[14] C. P. Race, J. von Pezold, and J. Neugebauer. Role of the mesoscale in migration kinetics of flat grain boundaries. *Physical Review B*, 89(21):214110, June 2014.

[15] A. Rajabzadeh, F. Mompiou, S. Lartigue-Korinek, N. Combe, M. Legros, and D.A. Molodov. The role of disconnections in deformation-coupled grain boundary migration. *Acta Materialia*, 77:223–235, September 2014.

[16] R. Hadian, B. Grabowski, M. W. Finnis, and J. Neugebauer. Migration mechanisms of a faceted grain boundary. *Physical Review Materials*, 2(4):043601, April 2018. Publisher: American Physical Society.

[17] R. Kobayashi, J. A. Warren, and W. C. Carter. Vector-valued phase field model for crystallization and grain boundary formation. *Physica D: Nonlinear Phenomena*, 119(3):415–423, August 1998.

[18] R. Kobayashi and Y. Giga. Equations with Singular Diffusivity. *Journal of Statistical Physics*, 95(5):1187–1220, June 1999.

[19] James A. Warren, Ryo Kobayashi, Alexander E. Lobkovsky, and W. Craig Carter. Extending phase field models of solidification to polycrystalline materials. *Acta Materialia*, 51(20):6035–6058, December 2003.

[20] Alexander E. Lobkovsky and James A. Warren. Sharp interface limit of a phase-field model of crystal grains. *Physical Review E*, 63(5):051605, April 2001.

[21] Alexander E. Lobkovsky and James A. Warren. Phase field model of premelting of grain boundaries. *Physica D: Nonlinear Phenomena*, 164(3):202–212, April 2002.

[22] Anna Ask, Samuel Forest, Benoit Appolaire, Kais Ammar, and Oguz Umut Salman. A Cosserat crystal plasticity and phase field theory for grain boundary migration. *Journal of the Mechanics and Physics of Solids*, 115:167–194, June 2018.

[23] Nikhil Chandra Admal, Giacomo Po, and Jaime Marian. A unified framework for polycrystal plasticity with grain boundary evolution. *International Journal of Plasticity*, February 2018.

[24] Cynthia L. Kelchner, S. J. Plimpton, and J. C. Hamilton. Dislocation nucleation and defect structure during surface indentation. *Physical Review B*, 58(17):11085–11088, November 1998. Publisher: American Physical Society.

[25] Christophe Denoual, Anna Maria Caucci, Laurent Soulard, and Yves-Patrick Pellegrini. Phase-Field Reaction-Pathway Kinetics of Martensitic Transformations in a Model Fe 3 Ni Alloy. *Physical Review Letters*, 105(3), July 2010.

[26] C. Reina, L. Sandoval, and J. Marian. Mesoscale computational study of the nanocrystallization of amorphous Ge via a self-consistent atomistic phase-field model. *Acta Materialia*, 77:335–351, September 2014.

[27] S Foiles and J Hoyt. Computation of grain boundary stiffness and mobility from boundary fluctuations. *Acta Materialia*, 54(12):3351–3357, July 2006.

[28] Murray S. Daw, Stephen M. Foiles, and Michael I. Baskes. The embedded-atom method: a review of theory and applications. *Materials Science Reports*, 9(7):251–310, March 1993.

[29] M. A. Tschopp and D. L. McDowell. Structures and energies of sigma 3 asymmetric tilt grain boundaries in copper and aluminium. *Philosophical Magazine*, 87(22):3147–3173, August 2007.

[30] Steve Plimpton. Fast Parallel Algorithms for Short-Range Molecular Dynamics. *Journal of Computational Physics*, 117(1):1–19, March 1995.

[31] Koenraad G. F. Janssens, David Olmsted, Elizabeth A. Holm, Stephen M. Foiles, Steven J. Plimpton, and Peter M. Derlet. Computing the mobility of grain boundaries. *Nature Materials*, 5(2):124–127, February 2006.

[32] A Acharya. Lattice incompatibility and a gradient theory of crystal plasticity. *Journal of the Mechanics and Physics of Solids*, 48(8):1565–1595, August 2000.

[33] Xiao-Yu Sun, Vincent Taupin, Patrick Cordier, Claude Fressengeas, and Bijaya B. Karki. Influence of pressure on dislocation, disclination, and generalized-disclination structures of a

{310}/[001] tilt grain boundary in MgO. *Journal of Materials Research*, 31(20):3108–3114, October 2016. Publisher: Cambridge University Press.

[34] F. J. H. Ehlers, M. Seydou, D. Tingaud, F. Maurel, S. Queyreau, and Y. Charles. Ab initio studies of two Al grain boundaries subjected to mixed tension/shear mode loading: how shear may promote breakage. *Modelling and Simulation in Materials Science and Engineering*, 25(6):064001, 2017.

[35] M. R. Gilbert, S. Queyreau, and J. Marian. Stress and temperature dependence of screw dislocation mobility in alpha -Fe by molecular dynamics. *Physical Review B*, 84(17):174103, November 2011.

[36] S. Queyreau, J. Marian, M. R. Gilbert, and B. D. Wirth. Edge dislocation mobilities in bcc Fe obtained by molecular dynamics. *Physical Review B*, 84(6), August 2011.